J. Fluid Mech. (2010), *vol.* 647, *pp.* 239–264.
doi:10.1017/S002211201000008X

The nonlinear dynamics of pendent drops on a thin film coating the underside of a ceiling

JOHN R. LISTER†, JOHN M. RALLISON AND SIMON J. REES

Institute of Theoretical Geophysics, Department of Applied Mathematics and Theoretical Physics, University of Cambridge, Wilberforce Rd, Cambridge CB3 OWA, UK

(Received 3 August 2009; revised 23 December 2009; accepted 28 December 2009)

This paper considers the dynamics of a thin film of viscous liquid of density ρ coating the underside of a horizontal rigid boundary under the action of surface tension σ and gravity g, and in the lubrication limit. Gravitational instability for inverse wavenumbers larger than the capillary length $\ell = (\sigma/\rho g)^{1/2}$ leads to the formation of quasi-static pendent drops of radius $\approx 3.83\ell$. If the boundary conditions are such as to pin the positions of the drops then the drops slowly drain fluid from the regions between them through thin annular trenches around each drop. A similarity solution is derived and verified numerically in which the film thickness in the intervening regions scales like $t^{-1/4}$ and that in the trenches like $t^{-1/2}$. A single drop placed far from boundaries on an otherwise uniform film, and given an initial perturbation, undergoes self-induced quasi-steady translation during which it grows slowly in amplitude by leaving a wake where the film thickness is reduced by an average of 90 %. It is driven by release of gravitational potential energy as fluid is collected from the film into the lower lying drop. Analysis of Landau–Levich regions around the perimeter of the translating drop predicts its speed and the profile of the wake. Two translating drops may coalesce if they collide, in contrast with the non-coalescence of colliding collars in the analogous one-dimensional problem (Lister *et al.*, *J. Fluid Mech.* vol. 552, 2006*b*, p. 311). Colliding drops may also bounce off each other, the outcome depending on the angle of incidence through complex interactions between their surrounding capillary wave fields.

1. Introduction

As sometimes observed on a kitchen or bathroom ceiling, a layer of liquid coating the underside of a rigid horizontal boundary is unstable and tends to accumulate into an array of pendent drops. If the initial layer is sufficiently thin then these drops do not drip off the ceiling, but remain supported in a near-equilibrium between surface tension and gravity. In this paper, we examine the nonlinear dynamics that govern the slow evolution and motion of such pendent drops, as they continue to accumulate fluid from the surrounding remnant thin film of liquid. A surprising result is that a single drop is capable of steady translation over an otherwise uniform horizontal film. In addition, we find that a colliding pair of translating drops may coalesce or may 'bounce' off each other, depending on the initial conditions. The nonlinear dynamics of pendent drops with two horizontal dimensions is significantly different from that

† Email address for correspondence: lister@esc.cam.ac.uk

found in the equivalent theoretical problem with one horizontal dimension (Lister *et al.* 2006*a*, *b*).

The initial instability of a layer of liquid to form drops is an example of Rayleigh–Taylor instability, which applies to any system where dense fluid overlies light. Linear stability analyses for a number of systems with two semi-infinite superposed layers are outlined in Chandrasekhar (1981, Chapter X). Many experimental and theoretical investigations of Rayleigh–Taylor instability for a finite-thickness, very viscous layer, without surface tension, have been motivated by geophysical applications (e.g. Nettleton 1934; Selig 1965; Whitehead & Luther 1975; Lister & Kerr 1989). The hexagonal planform observed in the nonlinear regime (e.g. Whitehead & Luther 1975) is relevant, for example, to geological formations of salt domes, which can trap oil and gas.

Linear stability analyses for the Rayleigh–Taylor instability of a finite-thickness viscous layer with surface tension, which is the system considered here, are discussed in some detail by Hynes (1978), Yiantsios & Higgins (1989) and Limat (1993). Independent of the initial layer depth $\hat{h}$ and the fluid-dynamic regime, a layer with surface tension is unstable to wavelengths greater than $2\pi\ell$, where $\ell = (\sigma/\Delta\rho g)^{1/2}$ is the capillary length, and σ is the surface tension and $\Delta\rho$ the (unstable) density difference across the interface between the layer and its environment.

Several studies of the weakly nonlinear development of the instability have focused on pattern formation in two horizontal dimensions. As in the case without surface tension, it is observed experimentally (Hynes 1978; Fermigier *et al.* 1992) that the preferred pattern of drops is hexagonal. Fermigier *et al.* (1992) show that this is the usual consequence of the lack of vertical symmetry – the rigid boundary above and free surface below – which leads to quadratic interaction terms in the weakly nonlinear amplitude equations for three perturbations at 120° to each other. Similar analysis can also be used with the Fourier decomposition of Bessel functions to explain the growth of axisymmetric disturbances around a point defect such as a speck of dust. Limat *et al.* (1992) and Fermigier *et al.* (1992) also examined experimentally the propagation of 'roll fronts' away from an edge of the fluid layer, or from a fine triggering wire, and the subsequent breakup of these fronts into a hexagonal pattern.

Studies of the long-term nonlinear evolution have largely been confined to just one horizontal dimension, with a domain of length $L > \pi\ell$ so that there is room for the linear instability to develop. Yiantsios & Higgins (1989) and Newhouse & Pozrikidis (1990) present numerical calculations for the case in which $\hat{h}/\ell$ is sufficiently large that, as the drops form, they accumulate a greater volume than the maximum possible in a pendent drop and begin dripping. If $\hat{h} \ll \ell$ then the liquid does not drip, but accumulates into a number of equilibrium drops of length $2\pi\ell$, separated by regions where the film thickness tends towards zero. The number and location of drops (or half-drops at the end of the domain) depends on L and the initial conditions (Yiantsios & Higgins 1989).

The nonlinear evolution for $\hat{h} \ll \ell$ can be described by lubrication theory, which yields a leading-order evolution equation identical in form to that derived by Hammond (1983) to describe (in the absence of gravity) the Rayleigh instability of an axisymmetric thin film of liquid coating the inside or outside of a rigid circular cylinder. In Hammond's problem the destabilizing effect of the azimuthal curvature takes the place of gravity and the radius of the cylinder takes the place of the capillary length. The Rayleigh instability leads to annular 'collars' (of length $2\pi a$, where a is the tube radius) and separating thin 'lobes' (of length less than $2\pi a$), which are

directly analogous to the pendent drops and separating thin regions later found by Yiantsios & Higgins (1989) in the one-dimensional Rayleigh–Taylor problem. Hammond (1983) also showed analytically, and numerically on domains of length $\sqrt{2}\pi\ell$ and $3\pi\ell$, that stationary lobes drain into neighbouring stationary collars through a quasi-steady neck of the kind identified by Jones & Wilson (1978). As a result, the thickness in the lobes decrease like $t^{-1/4}$ and the thickness in the necks like $t^{-1/2}$ at large times.

We note that, in practice, such drainage would eventually result in a sufficiently thin film that other effects such as surface roughness, intermolecular (e.g. van der Waals) forces or evaporation could become important. The subsequent dynamics might include rupture and dewetting (e.g. Zhang & Lister 1999; Fetzer *et al.* 2005) or the establishment of a nearly uniform ultra-thin film between slowly coarsening drops (e.g. Glasner & Witelski 2003; Gratton & Witelski 2008). We will assume that the film thickness is sufficient that the flow can be considered to be driven only by surface tension and gravity. Evaporation is neglected.

Both Hammond (1983) and Yiantsios & Higgins (1989) comment briefly that the behaviour on domains of length greater than $4\pi\ell$ may differ from that above since there is then room for one or more of the collars (drops) to translate in the interior of the domain. They were unable to investigate this further owing to the limitations of computational resources and methods at the time. Lister *et al.* (2006*b*) revisited Hammond's problem and used highly accurate finite-difference simulations, adaptive in both space and time, to uncover some complicated dynamics on longer domains. On such domains, a collar can episodically translate back and forth along the cylinder, on each occasion consuming the lobe ahead and leaving a smaller daughter lobe behind (figure 1). This motion takes place on several different time scales: the relatively rapid translation is governed by Landau–Levich equations; the collision of the translating collar with a neighbouring collar is governed by a new similarity equation for the neck regions ahead and behind in which the thickness varies like t^{-1}; and the delay between one episode of translation and the next is governed via the Landau–Levich equation by a slow peeling process in the daughter lobe. Asymptotic results for each of the processes of translation, collision and peeling were obtained and compared with a full numerical solution. Each episode of translation reduces the thickness of the daughter lobe by a factor ≈ 0.115, and successive translations back and forth give rise to a lobe thickness that decays on average and on very long time scales like $t^{-1/2}$ instead of the $t^{-1/4}$ obtained by the Hammond drainage mechanism. Some of these phenomena were rederived in Glasner (2007).

Two features of the energetics of this process are worth noting. First, the translation of a collar is driven by the factor of 0.115 reduction in the film thickness left behind the collar (through a Landau–Levich-like process): most of the film over which the collar passes is retained at lower pressure in the collar, thus leading to a decrease in the interfacial energy. Second, it would be energetically favourable for collars to coalesce when they collide and for the system to evolve towards a single large collar. This does not happen because the neck between colliding collars thins like t^{-1} as fluid is sucked into the collars, causing the forward motion of the collision to slow rapidly like $t^{-3/2}$, until a peeling process in the lobe on the other side of the collar eventually catches up and triggers a reversal of the motion.

The main purpose of the present paper is to examine how much of the behaviour found by Hammond (1983), Yiantsios & Higgins (1989) and Lister *et al.* (2006*a*, *b*) in one horizontal dimension carries over to two horizontal dimensions. In § 2 we

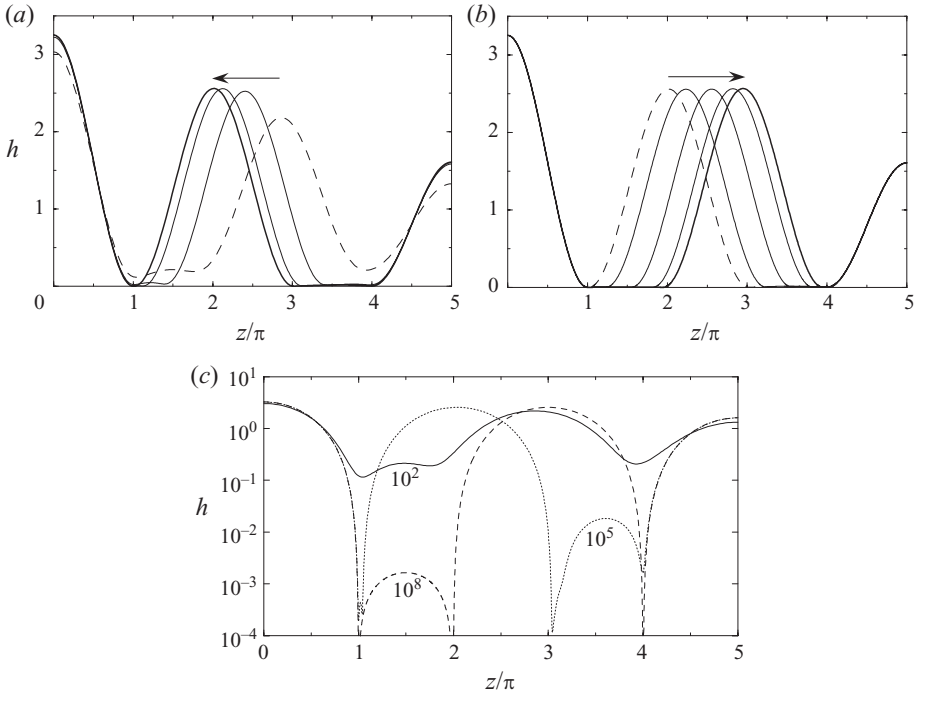

FIGURE 1. The evolution of a thin annular film of thickness h on a cylinder of length 5π taken from Lister *et al.* (2006*b*). (*a*) Time $t = 10^2$ (dashed), 10^3, 10^4 and 10^6 (bold); (*b*) $t = 2.1 \times 10^6$ (dashed), 2.18×10^6, 2.2×10^6, 2.22×10^6 and 2.3×10^6 (bold). Between $t = 10^2$ and 10^5 the central collar slides to the left from $2 < z/\pi < 4$ into $1 < z/\pi < 3$, consuming the lobe ahead of it and leaving a smaller daughter lobe ($h \sim 10^{-2}$) behind in $3 < z/\pi < 4$. Between $t = 2.1 \times 10^6$ and 2.3×10^6, the collar slides back to the right leaving an even smaller daughter lobe ($h \sim 10^{-3}$) in $1 < z/\pi < 2$. The episodic sliding motion is halted by collisions with the collars pinned at the ends of the domain by the boundary conditions and is reinitiated by a peeling process that cannot be seen on this scale. (*c*) The reduction in thickness of the lobe by a factor of about 10 by each sliding episode is shown on a logarithmic scale by profiles at $t = 10^2$ (solid), 10^5(dotted) and 10^8 (dashed).

formally define the problem, and show that the two-dimensional analogue of a collar is an axisymmetric drop of radius $\approx 3.8317\ell$. In § 3, we study the long-term evolution on a domain small enough that any drops are constrained to be stationary by the boundary conditions. We show that drainage of the intervening thin film into the drops can be described by a generalization of Hammond's analysis. In § 4 we show that on a larger domain a single drop can undergo quasi-steady translation over an otherwise uniform film, leaving a 'wake' in which the average thickness is less than that of the original film. Landau–Levich analyses around the perimeter of the drop are used together with a solubility criterion to predict the speed and direction of travel, and the variation in thickness across the wake. In § 5 we show that, in contrast to the non-coalescence of colliding collars, two drops will coalesce in a head-on collision. We also present illustrative calculations of off-set collisions of drops, and of the collision of a drop with a wake, showing how the trajectory of the translating drop is deflected. These situations have no one-dimensional analogue. We conclude with discussion of the challenge of observing a translating drop experimentally and with some open questions.

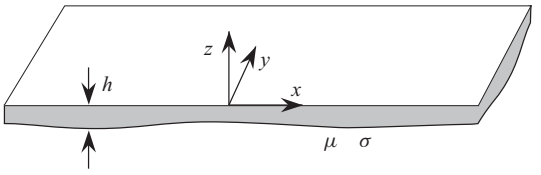

FIGURE 2. Definition sketch. The underside of a horizontal rigid boundary $z = 0$ is coated by a thin layer of liquid of viscosity μ, surface tension σ and thickness $h(x, y, t)$, where x and y are the horizontal coordinates.

2. Problem description

2.1. *Governing equation*

Consider a thin layer of liquid of density ρ, viscosity μ and thickness $h(x, y, t)$ coating the underside of a horizontal rigid boundary $z = 0$ (figure 2). We assume that the film thickness varies on a horizontal length scale much greater than h so that $|\nabla h| \ll 1$, where $\nabla = (\partial/\partial x, \partial/\partial y)$ denotes the horizontal gradient operator. It follows that the interfacial curvature is given by

$$\kappa = -\nabla^2 h\big(1 + O(|\nabla h|^2)\big). \tag{2.1}$$

We assume that both the external pressure p_0 and the surface tension σ are uniform. The flow in the film is then driven by horizontal gradients in the pressure

$$p = p_0 - \rho g(h + z) + \sigma\kappa \ , \tag{2.2}$$

which is derived from a vertical hydrostatic balance and the capillary jump across the interface. There is no slip at $z = 0$ and no tangential stress at $z = -h$. We assume that inertia is negligible and, using $|\nabla h| \ll 1$ again, make the usual lubrication approximations to obtain

$$h_t + \frac{1}{3\mu}\nabla \cdot \big(h^3\nabla(\rho g h + \sigma\nabla^2 h)\big) = 0. \tag{2.3}$$

Equation (2.3) also describes the evolution of a thin layer of fluid overlying a much deeper layer of less dense fluid, or underlying a deep layer of more dense fluid, provided ρ is replaced by the density difference between the layers and the viscosity of the deep layer is much less than $\mu/|\nabla h|$ (Yiantsios & Higgins 1989).

By scaling h in (2.3) with a typical initial thickness $\hat{h}$, x and y with the capillary length $\ell = (\sigma/\rho g)^{1/2}$, p with $\sigma\hat{h}/\ell^2$ and t with $\mu\ell^4/(\sigma\hat{h}^3)$, we obtain the dimensionless evolution equation

$$h_t + \tfrac{1}{3}\nabla \cdot \big(h^3\nabla(h + \nabla^2 h)\big) = 0. \tag{2.4}$$

This paper focuses on the evolution of solutions of (2.4) with two spatial variables x and y. The numerical calculations described in subsequent sections were performed on a finite domain $x_1 \leqslant x \leqslant x_2$, $y_1 \leqslant y \leqslant y_2$, subject to the symmetry (no-flux) boundary conditions

$$h_x = h_{xxx} = 0 \qquad (x = x_1,\ x_2), \qquad\qquad h_y = h_{yyy} = 0 \qquad (y = y_1,\ y_2). \tag{2.5}$$

As noted above, if there is only one spatial variable x, then (2.4) also describes the dimensionless evolution of a thin annular film of thickness $h(x, t)$ coating the inside or outside of a cylinder of radius $a \gg h$ in the absence of gravity (Hammond 1983; Lister *et al.* 2006*b*). In this context the second-derivative term in (2.4) arises from perturbations to the azimuthal curvature rather than gravity, the fourth-derivative

term arises from perturbations to the axial curvature, and x is made dimensionless with respect to the radius of the cylinder rather than the capillary length.

2.2. *Drop formation, energy and dissipation*

It is straightforward to show from (2.4) that a uniform film of thickness h_0 is linearly unstable on an infinite domain to wavevectors $\boldsymbol{k}$ with $k = |\boldsymbol{k}| < 1$ (e.g. Vrij 1966; Yiantsios & Higgins 1989), reflecting the long-wavelength Rayleigh–Taylor destabilization by gravity. The growthrate $(1/3)h_0^3k^2(1-k^2)$ has a maximum $h_0^3/12$ at $k = 2^{-1/2}$, reflecting the increase with wavelength in the viscous resistance to the lubrication flow.

The instability drives the film towards a state of lower energy E, where E is the sum of the gravitational potential energy and the interfacial energy. By expanding the relevant interfacial integral to $O(\hat{h}^2)$, consistent with the thin-film approximation (2.1), we find that

$$E = \frac{1}{2}\iint (|\nabla h|^2 - h^2)\,\mathrm{d}x\,\mathrm{d}y. \tag{2.6}$$

Subject to suitable boundary conditions, such as (2.5), periodicity or a uniform far-field thickness, it can be shown from (2.4) that $\mathrm{d}E/\mathrm{d}t = -\Phi$, where

$$\Phi = \frac{1}{3}\iint h^3|\nabla(h + \nabla^2 h)|^2\,\mathrm{d}x\,\mathrm{d}y \geqslant 0. \tag{2.7}$$

is the rate of dissipation in the thin-film approximation.

From (2.4) or (2.7), at each point of an equilibrium shape either $h = 0$ or $\nabla P = \boldsymbol{0}$, where

$$P = -(h + \nabla^2 h) \tag{2.8}$$

is the modified pressure. Equilibria thus consist of one or more regions, each of which has P uniform in its interior and $h = 0$ on any boundary. There are a wide variety of such solutions, found by solving (2.8) subject to these conditions.

The equilibrium solution of greatest importance to the rest of the paper, which we call a 'drop', is given by

$$h = A\left(1 + \frac{\mathrm{J}_0(r)}{J_R}\right), \quad (r \leqslant R) \qquad \text{and} \qquad h = 0 \quad (r > R), \tag{2.9}$$

where the amplitude A is a constant, r is the radial coordinate centred on any point in the x, y plane, J_0 is the regular Bessel function of order zero, $R \approx 3.8317$ is the first root of $\mathrm{J}_0'(R) = 0$, and $J_R = -\mathrm{J}_0(R) \approx 0.40276$. This solution contacts the plane tangentially at $r = R$. A drop is the axisymmetric analogue of the one-dimensional collar. The pressure in a drop is $-A$, the volume is $V = \pi R^2 A$ and the energy is $E = -\pi R^2 A^2/2 = -V^2/(2\pi R^2)$. With the boundary conditions (2.5), (2.9) can also describe a quarter drop in equilibrium in the corner of the domain or a half drop on an edge. With a small perturbation, the solution (2.9) for $r < R$ can be matched asymptotically to a surrounding much thinner film. We shall also use the term drop more loosely to describe the perturbed solution.

Another constant-pressure solution of (2.8) that contacts the plane tangentially is the two-dimensional extension of the collar solution into a strip with

$$h = A(1 + \cos z), \quad (|z| \leqslant \pi) \qquad \text{and} \qquad h = 0 \quad (|z| > \pi), \tag{2.10}$$

where z is the coordinate perpendicular to any line in the x, y plane. When subject to the no-flux boundary conditions (2.5), the line must be parallel to one of the axes,

and (2.10) also describes an equilibrium half strip when the line is one edge of the domain.

Drops and strips (including the variants at corners and edges) are the only equilibrium solutions we know that have entirely tangential contact, though we have not proved that no other solutions exist. There are many solutions that meet the plane at a non-zero angle, which are the two-dimensional analogues of lobes. Indeed, given any bounded region in the plane, there is a unique solution to the Helmholtz problem $\nabla^2 h + h = 1$ in the region subject to $h = 0$ on its boundary. Provided $h > 0$ throughout the region, which implies that $\partial h/\partial n \leqslant 0$ on the boundary, this gives a valid lobe-like equilibrium. As we shall see in § 3, on a sufficiently small domain the film evolves towards a number of drops surrounded by a much thinner lobe-like region.

2.3. *Choice of numerical method*

Lister *et al.* (2006*b*) found that the long-term evolution of the one-dimensional solutions of (2.4) is controlled by very thin regions of the film (necks) that connect much thicker regions of the film (collars or lobes). Owing to the large contrast in the values of the mobility coefficient h^3, the evolution of the thin necks occurs on a much longer time scale than that of adjustment of the collars and lobes to their equilibrium shapes. For large times t, the evolution of the necks is typically self-similar with time scale $O(t)$, whereas the adjustment time scale of the collars remains $O(1)$ so that they are in almost static equilibrium.

Any explicit discretization of (2.4) would be crippled by infeasibly small time steps for stability. A fully implicit method requires iterative solutions of nonlinear equations, and it is not always clear (see comments below) whether the effective dynamics of iteration will match the very stiff dynamics of the late-time film evolution. Lister *et al.* (2006*b*) found that it was possible to calculate the long-term evolution accurately and efficiently in one dimension, by using a semi-implicit method in which the mobility coefficient h^3 was represented explicitly, but the film pressure (which is constant within the quasi-static collars and lobes) was represented fully implicitly. Thus the collars and lobes relax to the correct equilibria even if large time steps, proportional to t, are taken to follow the slow self-similar evolution of the necks.

The semi-implicit method for (2.4) can be written

$$h^{(n+1)} - h^{(n)} = -\tfrac{1}{3}\big(t^{(n+1)} - t^{(n)}\big)\nabla \cdot \big(f\big(h^{(n)}\big)\nabla\big(\nabla^2 h^{(n+1)} + h^{(n+1)}\big)\big), \tag{2.11}$$

where $h^{(n)}$ is the film thickness at time t^n and $f(h) = h^3$. In one dimension, spatial discretization of the right-hand side of (2.11) gives an easily solvable pentadiagonal system for $h^{(n+1)}$. In two dimensions, spatial discretization with a 13-point computational molecule gives rise to a large sparse non-symmetric banded matrix. In an attempt to preserve the advantages of the one-dimensional method, we tried evolving (2.11) using a bi-conjugate gradient method with a variety of preconditioners to obtain a good approximate inversion of the banded matrix. Unfortunately, as described in more detail in the Appendix, we found that the algorithm ran into difficulties as the film-thickness variations increased and the matrix became increasingly ill-conditioned.

Instead, we computed the results that follow using an operator-splitting alternating direction implicit (ADI) method, adapted from one of the methods proposed by Witelski & Bowen (2003). In our implementation, the terms that involve only x-derivatives or only y-derivatives (in particular, h_{xxxx} and h_{yyyy}) are treated by ADI, while the mixed-derivative terms (in particular, h_{xxyy}) and the mobility coefficient

are treated explicitly. The details are given in the Appendix. This method allows time steps of order unity, but cannot maintain the self-similar speed-up because the operator splitting that separates the x and y directions involves errors of order Δt^2. (As an aside, Witelski & Bowen 2003 use Neumann stability analysis to show that the ADI scheme gives unconditional numerical stability of perturbations to a uniform film when the second-order destabilizing term is not present. We found that the ADI scheme was unstable at large Δt^2 when the film is far from uniform.)

The majority of our calculations were performed on a fixed, evenly spaced rectangular grid with spacings Δx and Δy typically about 0.04. For one-dimension, Lister *et al.* (2006*b*) used adaptive grid spacing to resolve the very short and decreasing length scales of the necks out to times of order 10^{10}. In two-dimensions it is not possible to do so without losing the advantages of a regular grid. Our simulations were thus limited by resolution of the decreasing length scales, as well as by time step, to times of order 10^6, and both the spatial discretization and the time-stepping algorithm would need overhauling to do significantly better. The accuracy of the numerical scheme for the results reported here has been checked by varying the grid spacing, the time step and, where relevant in § 4, the domain size.

3. Drop formation and drainage on a small domain

3.1. *Simple geometric considerations*

Consider the evolution of (2.4) on the rectangular domain $0 \leqslant x \leqslant L_x$, $0 \leqslant y \leqslant L_y$ subject to the boundary conditions (2.5) in which $x_1 = y_1 = 0$, $x_2 = L_x$ and $y_2 = L_y$. If L_x and L_y are sufficiently small then the solution is constrained by the boundary conditions to be fairly straightforward. The following geometric considerations are supported by sample numerical calculations with various initial conditions and values of L_x and L_y.

If $L_x < \pi$ and $L_y < \pi$ then there is no room for an unstable wavelength and the solution evolves towards a uniform film (provided there is no initial dry patch).

If $L_x > \pi$ or $L_y > \pi$ then a uniform film is unstable to a general perturbation, which then evolves towards a number of equilibrium solutions of the form (2.9) or (2.10) – drops or strips – separated by much thinner regions. On a small domain there is only room for a small number of drops or strips, and these are constrained to form in the corners or along the sides of the domain, where they are pinned by the boundary conditions. On such a domain the long-term behaviour is largely determined by the values of L_x and L_y, and only to a lesser extent by the initial conditions.

If at least one of L_x or L_y is less than $R \approx 3.83 > \pi$ and at least one of them exceeds π then the domain is too narrow to accommodate even a quarter of the drop solution (2.9), but a uniform film is nevertheless unstable. In this case, the film will evolve towards strips spanning the domain in one direction, usually the shorter, and the subsequent dynamics in the perpendicular direction is very similar to that of the one-dimensional problem. For example, figure 3 shows stages in the evolution of the film for $L_x = 3\pi$, $L_y = 1.1\pi \approx 3.5 < R$ and initial condition

$$h(x, y, 0) = 1 + 0.01\cos(\pi x/L_x) + 0.1\cos(\pi y/L_y). \tag{3.1}$$

This domain is sufficiently large that a uniform film is unstable in both the x and y directions. The initial condition is such as to excite flow primarily in the y direction (figure 3*a*), and there would be room for a half-strip solution of the form $A(1+\cos y)$ in $0 \leqslant y \leqslant \pi$. However, instability in the x direction causes the film to veer away from

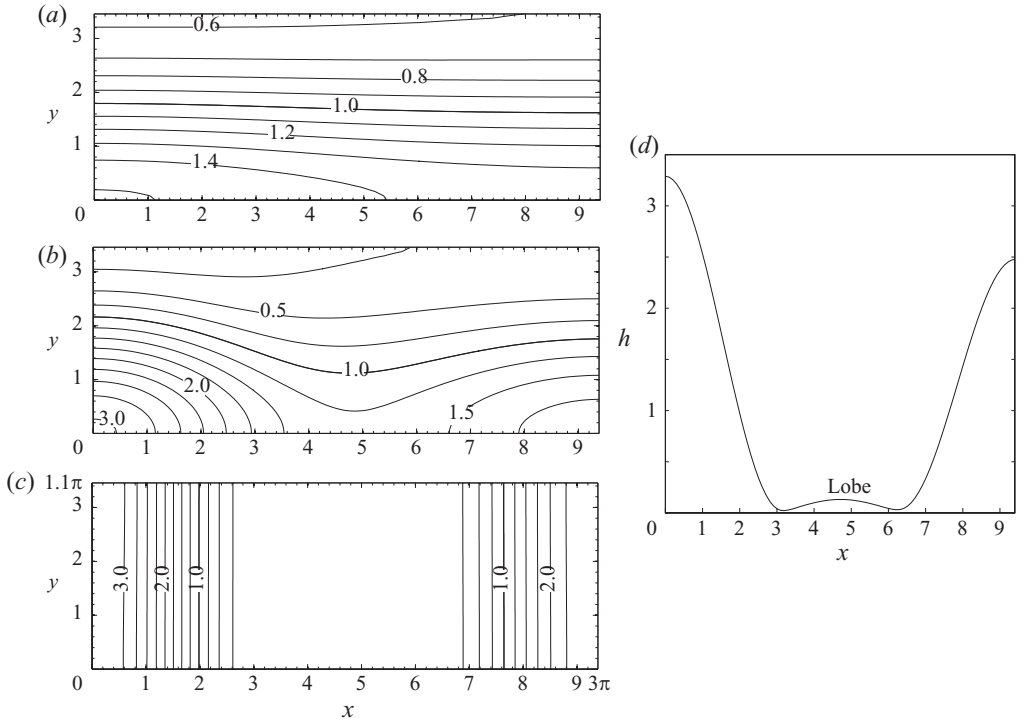

FIGURE 3. Evolution from initial condition (3.1) with $L_x = 3\pi$, $L_y = 1.1\pi \approx 3.5 < R$. (*a*)–(*c*) Contour plots of h at $t = 32$, 64 and 1024. (*d*) $h(x, 0)$ at $t = 1024$. Growth of the initial perturbation in the y direction towards a half-strip (*a*) is destabilized by the growth of variations in the x direction (*b*). The lack of room for a quarter drop in the corners then leads to the development of an approximately one-dimensional structure with a pinned half-strip at each end (*c*,*d*). The lobe in $\pi < x < 2\pi$ is draining into the adjacent half-strips.

a half-strip solution and towards quarter drops in two corners (figure 3*b*). However, since there is insufficient room in the y direction for quarter drops, the film makes a further transition towards an almost one-dimensional structure (figure 3*c*) in which flow is in the x direction and a thin central lobe drains into half-strips pinned at each end (cf. figure 3*c* of Lister *et al.* 2006*b*). If $L_y < R$ and $L_x > 4\pi$ then there is also room for a central strip of width 2π to oscillate between the pinned half-strips of width π by the processes of translation, collision and peeling described in Lister *et al.* (2006*b*).

If $R \leqslant L_x < 2R$ and $R \leqslant L_y < 2R$ then there is room either for a quarter drop in one corner of the domain, or for two quarter drops in opposite corners, but no room for a complete drop or half drop. (Two quarter drops require $L_x^2 + L_y^2 \geqslant 4R^2$.) It is also possible for there to be no room for complete or half drops on somewhat larger domains (e.g. up to $L_x^2 + L_y^2 = 16R^2$ for complete drops) if quarter drops already occupy some or all of the corners. In all these restricted configurations, once quarter drops have formed in the corners, the subsequent drainage of the intervening thin film into the quarter drops can be described by an extension of the analysis of Jones & Wilson (1978) or Hammond (1983). We first present a numerical calculation for a particular case in § 3.2 and then describe the general theory in § 3.3.

The dynamics of drops for yet larger values of L_x and L_y is discussed in §§ 4 and 5.

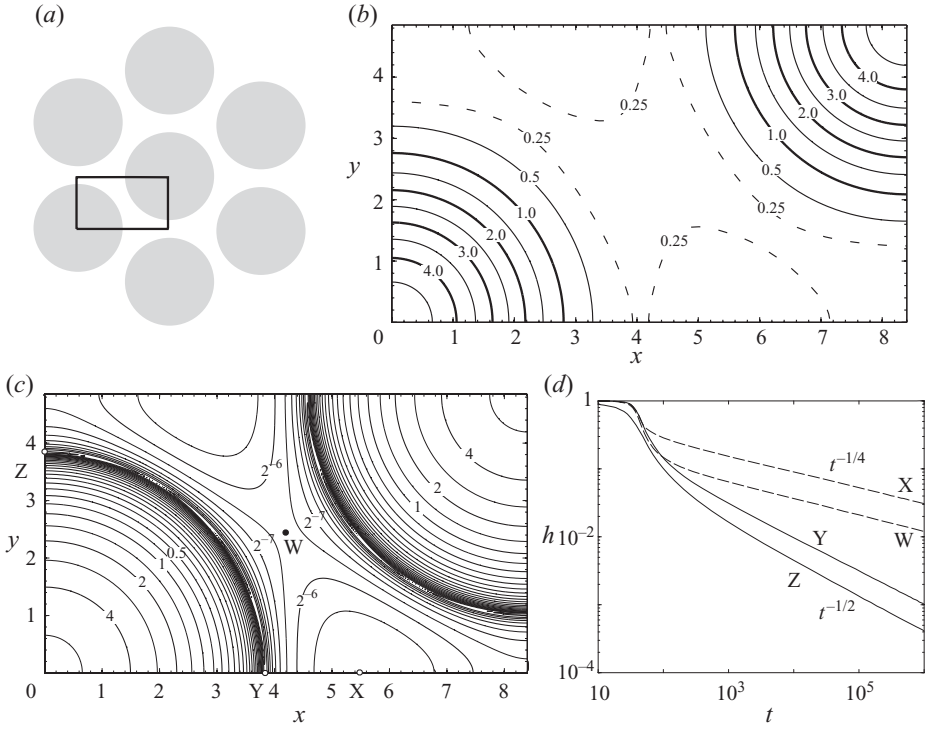

FIGURE 4. (*a*) A simulation with $L_x/L_y = \sqrt{3}$ can be considered part of a periodic hexagonal array of drops. (*b*) Contour plot of h at $t = 64$ for $L_x = 8.4$, $L_y = 4.85$ and initial condition (3.2). (*c*) Contour plot of $\log_2 h$ at $t \approx 10^6$ showing the quarter drops in two corners, the deep trenches around their edge and the draining lobe-like region in the middle. (*d*) The time-dependence of various heights in the domain. The minima along the x and y axes in the trench (points Y and Z) have $h \sim t^{-1/2}$. The heights at the centre of the domain (W) and at the local maximum at $(x, y) \approx (5.5, 0)$ (X) both have $h \sim t^{-1/4}$ (dashed). (The white patches in the trench are a graphical artefact.)

3.2. *Numerical example of drainage*

Our illustrative calculation is the case $L_x = 8.4$, $L_y = 4.85$ with initial condition

$$h(x, y, 0) = 1 + 0.05\cos(\pi x/L_x)\cos(\pi y/L_y). \tag{3.2}$$

These values of L_x and L_y were chosen so that quarter drops have room to form in two diagonally opposite corners and also so that $L_x/L_y = 1.7320 \approx \sqrt{3}$. The calculation can thus be considered to be simulation of drainage into a periodic hexagonal array of drops (figure 4*a*). Such an array has been observed experimentally and is predicted by weakly nonlinear analysis (Fermigier *et al.* 1992). The wavelength of the array here, $\lambda \approx 9.7$, was chosen to be a little larger than that of the most rapidly growing mode, $2\pi\sqrt{2} \approx 8.9$, in order to increase the minimum separation $\lambda - 2R$ between the drops and reduce the cost of a resolved calculation.

By $t = 64$ most of the fluid in the film has accumulated into two drops in opposite corners of the domain (figure 4*b*). The structure of the solution for longer times can be seen in a contour plot of $\log h$ at $t = 2^{20} \approx 10^6$ (figure 4*c*). The drops are surrounded by circular 'trenches', where the film is very thin and which separate the drops from a less thin film in the remaining region between the drops. Figure 4(*d*) shows the time-dependence of the film thickness at two points in the region between

the drops and three points in one of the trenches. At large times these thicknesses vary like $t^{-1/4}$ and $t^{-1/2}$, respectively. These scalings are the same as those found by Hammond (1983) for the drainage of a lobe through a thin neck into a neighbouring collar. We infer that the region between the drops is analogous to a lobe, the trench to a neck and the drop to a collar.

3.3. *Theory for drainage*

Consider a situation in which quarter drops form in at least one corner of the rectangular domain $0 \leqslant x \leqslant L_x$, $0 \leqslant x \leqslant L_y$ and where there is no room for any other drops to form. At large times, a narrow trench around each quarter drop controls the flux into that drop from a slowly draining lobe-like region between the drops. The film is much thinner in the trench than in the drops or the lobe, which has several consequences: (i) The volume of fluid in the trench can be neglected in comparison to that in the drops and the lobe. (ii) Drainage is much slower than the adjustment times of the drops and the lobe, which are thus in quasi-static equilibrium and have uniform pressures at leading order. (iii) The solutions for the drops and the lobe satisfy $h = 0$ at leading order along the circular arcs where they meet in a trench.

Each quarter drop thus takes the form (2.9) for $0 \leqslant \phi \leqslant \pi/2$, where (r, ϕ) are local polar coordinates centred on the relevant corner. We write the amplitude of drop i as $A_i(t)$. The lobe occupies a region $\mathscr{A}$ that is the rectangular domain minus the regions occupied by the quarter drops. It is thus bounded partly by the circular arcs $r = R$ at the edge of the drops and partly by some of the edges of the rectangular domain. Taking the uniform pressure in the lobe as $-P(t)$ and using (2.8), the leading-order solution for the film thickness within the lobe is $h(x, y, t) = P(t) f(x, y)$, where $f(x, y)$ is the unique solution of the Helmholtz problem

$$\nabla^2 f + f = -1 \text{ in } \mathscr{A}, \quad f = 0 \text{ at edges of drops}, \quad \partial f/\partial n = 0 \text{ at edges of domain}. \tag{3.3}$$

The volume of the lobe is $V_0 P(t)$, where $V_0 = \int_{\mathscr{A}} f \, dx \, dy$, and the slope of the lobe as it approaches the trenches around each drop is $\Theta_i(\phi) P(t)$, where $\Theta_i(\phi) = \partial f/\partial r|_{r=R+}$.

From volume conservation

$$\tfrac{1}{4}\pi R^2 J_R \frac{\mathrm{d}A_i}{\mathrm{d}t} = \int_0^{\pi/2} q_i(\phi, t)\, \mathrm{d}\phi \quad \text{and} \quad V_0 \frac{\mathrm{d}P}{\mathrm{d}t} = -\sum_i \int_0^{\pi/2} q_i(\phi, t)\, \mathrm{d}\phi, \tag{3.4}$$

where $q_i(\phi, t)$ denotes the flux from the draining lobe across each trench into the adjoining drop. As we shall see, the q_i decrease rapidly like $t^{-5/4}$ so that the A_i tend to constant values, which depend on the initial distribution of fluid. What remains is to determine the actual fluxes $q_i(\phi, t)$ by matching a solution for a trench to the drop on one side and the lobe on the other.

Because the trenches are narrow, the leading-order flux in the trench is radial, independent of r across the trench, and given by $q_i(\phi) = -h^3 h_{rrr}/3$. The matching conditions to the lobe and the drop are $h \to (r - R)\theta$ as $r - R \to \infty$ and $h \to (1/2)A_i(r - R)^2 + O(1)$ as $r - R \to -\infty$, where $\theta = \Theta_i(\phi) P(t)$ is the slope of the lobe and A_i is the basal curvature of the drop. (The limits $r - R \to \pm\infty$ are interpreted in the usual asymptotic sense corresponding to the overlap between inner and outer solutions.) By setting $h = 3q_i\theta^{-3}H$ and $r - R = -3q_i\theta^{-4}X$, we can rescale the equations at each ϕ and for each i onto the canonical problem:

$$H^3 H''' = 1, \qquad H \sim -X \text{ as } X \to -\infty, \qquad H \sim \tfrac{1}{2}\mathscr{C} X^2 \text{ as } X \to \infty, \tag{3.5}$$

where $\mathscr{C} = 3q_i(\phi)A_i\theta^{-5}$. As noted by Jones & Wilson (1978) and Hammond (1983), the problem (3.5) only has a solution for a particular value of $\mathscr{C}$, namely $\mathscr{C} \approx 1.2098$ (Jensen 1997). Thus

$$q_i(\phi, t) = \tfrac{1}{3}\mathscr{C}\theta(\phi, t)^5/A_i \ . \tag{3.6}$$

We combine this local analysis of the trench with (3.4) to obtain the drainage equation

$$\frac{\mathrm{d}P}{\mathrm{d}t} = -\tfrac{1}{4}P^5\left(\frac{4\mathscr{C}}{3V_0}\sum_i A_i^{-1}\int_0^{\pi/2}\Theta_i^5(\phi)\,\mathrm{d}\phi\right). \tag{3.7}$$

Clearly $P(t) = \{k(t-t_0)\}^{1/4}$, where k is the term in parentheses in (3.7) and t_0 is a constant of integration. The constant k depends on the shape of $\mathscr{A}$ through the solution of (3.3) and on the amplitudes A_i of the drops.

It follows from (3.7) and the Jones–Wilson solution (3.5) in the trench that the typical film thickness in the trenches scales like $t^{-1/2}$, the trench widths and film thickness in the lobe both scale like $t^{-1/4}$ and the fluxes q_i scale like $t^{-5/4}$. These scalings are all in agreement with the numerics in § 3.2.

4. Translation of a drop over a uniform layer

If the domain is larger than those considered in the previous section (e.g. $L_x, L_y > 2\sqrt{2}R$), then there is room for at least one drop to form in the interior of the domain where it is not pinned by the boundary conditions. The dynamics are then more complicated than the drainage into stationary drops described above.

We consider first the simplest case of a single drop on an otherwise uniform infinite layer. We show that, given an initial perturbation, the drop undergoes self-induced quasi-steady translation over the uniform layer, grows slowly in amplitude and leaves a wake where the film thickness is reduced. We illustrate with a numerical calculation, and then present a theoretical analysis of translation based on the controlling influence of Landau–Levich regions around the edge of the drop.

4.1. *Numerical example of translation*

We solved (2.4) numerically subject to the initial conditions

$$h = f(\tilde{r}) + 0.020 + 0.005\sin(\pi\tilde{x}/6) \qquad (|\tilde{x}| \leqslant 3), \tag{4.1a}$$

$$h = 0.020 + 0.005\,\mathrm{sgn}(\tilde{x}) \qquad (|\tilde{x}| \geqslant 3). \tag{4.1b}$$

where $\tilde{x} = x - 4.5$, $\tilde{r}^2 = \tilde{x}^2 + y^2$, and $f(\tilde{r})$ is the solution for a drop of unit height, i.e. (2.9) with amplitude $A = J_R/(J_R+1)$ so that $f(0) = 1$. This prescription gives a drop of unit height initially centred on (4.5, 0) and sitting on a fluid layer of thickness chosen to act as a smooth 'ramp' that leads to a layer of uniform thickness $h_+ = 0.025$ in $x \geqslant 7.5$. The calculations were done with $0 \leqslant y \leqslant 20$, but we use the symmetry about $y = 0$ implied by the boundary conditions (2.5) to show the solution in $-20 \leqslant y \leqslant 20$.

After a short transient, the difference in height across the ramp initiates motion of the drop in the x direction. By $t = 7 \times 10^5$ the centre of the drop has travelled well away from from the ramp to $x = 25$ (figure 5*a*) and a wake, where the film thickness is significantly less than h_+, extends from the drop back to its starting position. The central height of the drop, $h_d(t)$, has increased to about 1.32 owing to the fluid removed from the wake.

In order to study indefinite translation with a finite computational domain $x_1 \leqslant x \leqslant x_2$, we adopted the simple strategy of incrementing both x_1 and x_2 by 10 (with

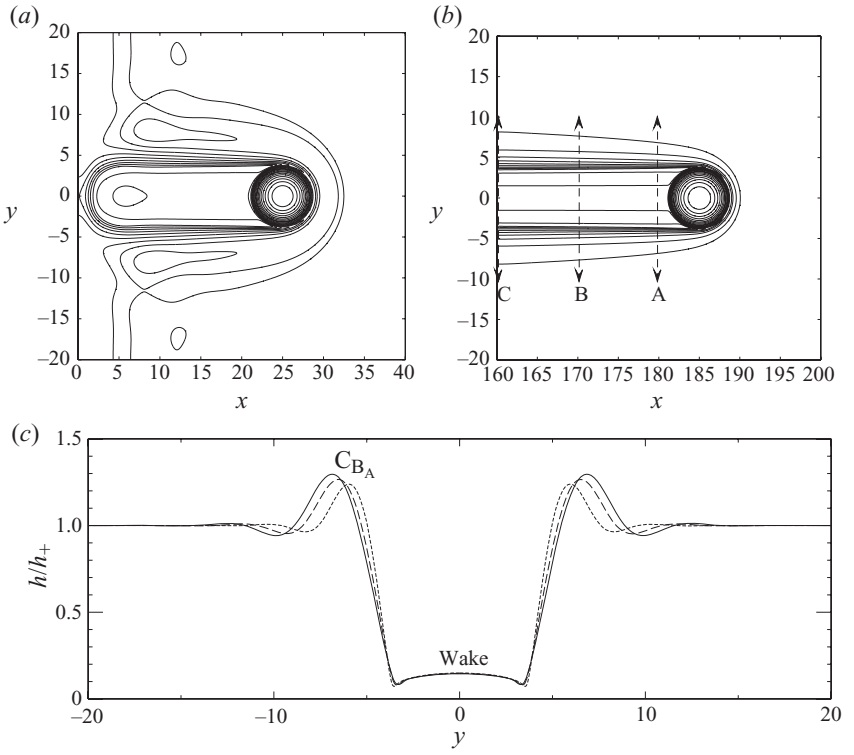

FIGURE 5. A translating drop. (*a*) Initial motion triggered by a small step. (*b*) Quasi-steady translation. (*c*) Cross-sections through the wake along the lines marked in (*b*).

$x_2 - x_1 = 40$) whenever the centre of the translating drop reaches $x = x_2 - 15$. The film thickness in the new region ahead of the drop is set to h_+, and the region more than 15 behind the drop is discarded. This change to the domain has only a slight effect on the solution near the boundaries and causes negligible disturbance to the solution near the drop and in the wake.

In figures 5(*b*) and 5(*c*), we show the quasi-steady structure of the wake after the drop has propagated many times its own radius. In the region $|y| < R$ directly behind the drop, we see that the film thickness varies across the wake, but very little along the wake, and can thus be approximated as a function $h_-(y)$. We note that $h_-(y) < 0.15h_+$. Since the mobility coefficient in (2.4) is h^3, the evolution in this wake is extremely slow and h_- is determined by the thickness left behind the trailing edge of the drop. On either side of the wake there is a capillary ridge of height about $1.2h_+$, which is shed from the sides of the drop and spreads slowly in the y direction away from the wake.

After the initial transient, the amplitude increases linearly with distance (not shown) and the speed c of the drop increases with its amplitude (figure 6*a*). Integration across the wake profiles (figure 5*c*) provides an alternative measure of the fluid accumulated by the drop. The quantitative results, and those from similar calculations with $h_+ = 0.01$, are well represented by the equations

$$c = \alpha(h_+h_d)^{3/2}\{1 + 2.04(h_+/h_d)^{1/2}\}, \qquad \alpha = 0.00485, \tag{4.2}$$

$$\mathrm{d}h_d/\mathrm{d}x = \beta h_+, \qquad \beta = 0.52, \tag{4.3}$$

$$\int_0^\infty (h_+ - h_-)\,dy = \gamma h_+ R, \qquad \gamma = 0.90. \tag{4.4}$$

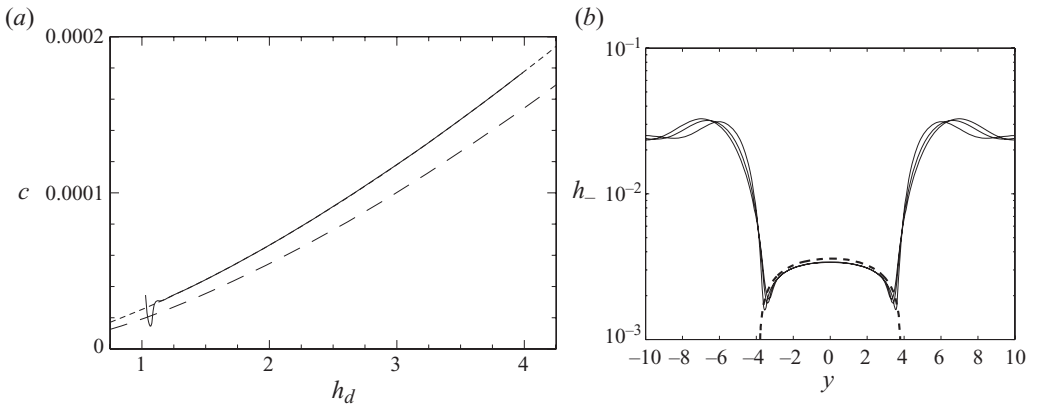

FIGURE 6. (*a*) The growth in translation speed c with drop height h_d for the numerical calculation in § 4.1 (solid). After a short transient, there is an almost perfect fit with the form $c = c_0 h_d^{3/2} + c_1 h_d$ (short dashed), where $c_0 = 1.92 \times 10^{-5}$ and $c_1 = 0.62 \times 10^{-5}$. The theoretical prediction (4.20) is shown long dashed. (*b*) Comparison of the profiles across the wake (solid) with the theoretical prediction (4.13*a*, dashed).

4.2. *Theory for translation*

We seek a quasi-steady travelling-wave solution of (2.4) to describe a drop of slowly varying amplitude $A(t)$ travelling with speed $c(t)$ in the x direction over a uniform layer of much smaller prescribed thickness h_+.

If the drop leaves behind a wake of smaller thickness $h_-(y)$ then the volume of the drop increases at a rate

$$\frac{\mathrm{d}V}{\mathrm{d}t} = c\int (h_+ - h_-)\,\mathrm{d}y \quad \text{or} \quad \frac{\mathrm{d}V}{\mathrm{d}x} = \int (h_+ - h_-)\,\mathrm{d}y, \tag{4.5}$$

where $V = \pi R^2 A$. Hence if $\delta \equiv (h_+/A)^{1/2} \ll 1$ then the growth of the drop is slow on the time scale of propagation over its own length, and the solution is quasi-steady in the frame of the drop.

Let (x, y) or (r, θ) be coordinates centred on the moving drop (so $\theta = 0$ is the direction of motion). Then

$$\nabla \cdot \left(h^3 \nabla (h + \nabla^2 h)\right) = 3ch_x + O(\delta^2 ch), \tag{4.6}$$

where $O(\delta^2 ch)$ terms arise from the fact that the amplitude of the drop is slowly varying.

In the drop $h = O(1)$ and $p = -h - \nabla^2 h$ is approximately constant. Anticipating the scaling $c = O(\delta^3)$, we posit a quasi-steady drop shape

$$h = A(\mathrm{J}_0(r)/J_R + 1) + B(r, \theta) + O(\delta^3), \tag{4.7}$$

where $B(R, \theta) = O(h_\pm) = O(\delta^2)$.

Around the drop we expect a narrow ring of size $O(\delta)$ where the curvature changes rapidly in order to match the edge of the drop to the thin films. This matching region is analogous to those found in the Landau–Levich and Bretherton problems (Landau & Levich 1942; Bretherton 1961). Except at the sides of the drop ($\theta = \pm\pi/2$), we expect the radial variations in curvature to be dominant and hence, at leading order, (4.6) becomes

$$(h^3 h_{rrr})_r = (3c\cos\theta)h_r. \tag{4.8}$$

By defining rescaled variables

$$h = h_{\pm} H_{\pm}(\xi), \quad \text{where} \quad \xi = (3c\cos\theta)^{1/3}(r - R)/h_{\pm}, \tag{4.9}$$

and integrating (4.8) once, we obtain the Landau–Levich equation

$$H^3 H''' = H - 1. \tag{4.10}$$

This equation has a unique solution $H_-(\xi)$ with

$$H_- \to 1 \quad \text{as} \quad \xi \to -\infty, \qquad H_- \sim \tfrac{1}{2}a_-\xi^2 + b_- \quad \text{as} \quad \xi \to \infty, \tag{4.11}$$

where $a_- = 0.6430$ and $b_- = 2.8996$, and a one-parameter set of solutions $H_+(\xi;\lambda)$ labelled by λ with

$$H_+ \to 1 \quad \text{as} \quad \xi \to \infty, \qquad H_+ \sim \tfrac{1}{2}a_+(\lambda)\xi^2 + b_+(\lambda) \quad \text{as} \quad \xi \to -\infty. \tag{4.12}$$

We note that h_+ is given and $h_-(\theta)$ is to be found.

Towards the edge of the drop shape (4.7) the radial curvature h_{rr} approaches the value A. This curvature must match the quadratic terms in the asymptotic behaviour of $H_\pm$ as $\xi \to \mp\infty$. Thus, given c, we can use (4.9) and (4.11*b*) to predict the rear profile

$$h_-(\theta) = a_- A^{-1}(3c\cos\theta)^{2/3}\ . \tag{4.13}$$

Again given c, we can use (4.9) and (4.12*b*) to find $\lambda(\theta)$ from

$$a_+(\lambda) = h_+ A(3c\cos\theta)^{-2/3}, \tag{4.14}$$

and hence also find $b_+(\theta)$.

Furthermore, matching the constant terms in the asymptotic behaviour of $H_\pm$ to the drop shape (4.7) determines the vertical offset $B(R,\theta)$ at the front and the back of the drop in terms of the surrounding film thickness:

$$B_-(\theta) = h_-(\theta)b_-, \qquad B_+(\theta) = h_+ b_+(\lambda). \tag{4.15}$$

At $O(\delta^2)$, (4.6) suggests that the drop has uniform pressure, and hence that it satisfies $\nabla^2 h + h = const.$ subject to $h \sim B(\theta) + (1/2)A(R - r)^2$ as $r \to R$. This Helmholtz problem can be solved by separation of variables, provided the Fourier series for $B(\theta)$ does not include a term proportional to $\cos\theta$. (Note that the Helmholtz solution $\mathrm{J}_1(r)\cos\theta$ cannot satisfy an inhomogeneous boundary condition at $r = R$, since $\mathrm{J}_1(R) = 0$. The corresponding orthogonality to $\sin\theta$ is guaranteed by symmetry.) The absence of a term proportional to $\cos\theta$ provides the solubility criterion

$$\int_0^{\pi} B(\theta)\cos\theta\,\mathrm{d}\theta = 0, \tag{4.16}$$

which determines c as follows.

For convenience, let

$$C = (3c)^{2/3}/(Ah_+) \tag{4.17}$$

so that (4.13) and (4.14) become $h_-(\theta) = a_- C(\cos\theta)^{2/3}h_+$ and

$$a_+(\lambda) = [C(\cos\theta)^{2/3}]^{-1}. \tag{4.18}$$

The speed is found from (4.16) by solving

$$Ca_-b_- \int_0^{\pi/2} (\cos\theta)^{2/3}\cos\theta\,\mathrm{d}\theta = \int_0^{\pi/2} b_+[\lambda(\theta, C)]\cos\theta\,\mathrm{d}\theta \tag{4.19}$$

for C, where $\lambda(\theta;C)$ is given by (4.18).

Numerical solution of (4.18) and (4.19) gives $C = 0.2086$. Substitution into (4.17) and (4.13) yields

$$c = \tfrac{1}{3}(CAh_+)^{3/2} = 0.0318(Ah_+)^{3/2}, \tag{4.20}$$

$$\int_{-R}^{R} h_- \,\mathrm{d}y = h_+ R\, Ca_- \int_{-\pi/2}^{\pi/2} (\cos\theta)^{2/3} \cos\theta \,\mathrm{d}\theta = 0.2257 h_+ R\ . \tag{4.21}$$

These predictions agree well with the scalings and numerical coefficients from the numerical simulation. Using $h_d = A(J_R^{-1} + 1)$ in (4.20), we predict $\alpha = 0.004886$ in (4.2) which compares to the fitted value 0.00485 from the simulation. From (4.21) we predict $\gamma = 0.8872$ in (4.4) which compares to the fitted value 0.90. By mass conservation we predict $\beta = 2\gamma(J_R^{-1} + 1)/(\pi R) = 0.5133$ in (4.3) which compares to the fitted value 0.52.

The speed observed in the simulation (figure 6*a*) differs by about 20 % from the asymptotic prediction (4.20) over the range of h_d calculated, this difference being almost entirely accounted for by the $2.04(h_+/h_d)^{1/2}$ correction in (4.2). This correction is $O(\delta)$, as might be expected from the ratio of the width of the Landau–Levich regions to the radius of the drop. The profile of $h_-(y)$ $(-R \leqslant y \leqslant R)$ in the calculated wake (figure 6*b*) agrees well with the predicted $(\cos\theta)^{2/3}$ profile from (4.13) except close to the edges of the wake, which are shed from the sides of the drop.

At the sides of the drop ($\theta \approx \pm\pi/2, \cos\theta \approx 0$) there are small regions where the Landau–Levich analysis breaks down and the azimuthal variations are as important as the radial variations. An adaptation of the analyses of Burgess & Foster (1990) for a bubble in a Hele-Shaw cell, and of Hodges, Jensen & Rallison (2004) for a drop sliding down an inclined plane, shows that these regions should subtend an $O[(h_+R^2/A^3)^{3/10}]$ angle and occupy a lateral width $\Delta y = O[R(h_+R^2/A^3)^{3/5}]$. If $A = O(1)$ and $h_+ = O(\delta^2)$, as assumed, then this angle is $O(\delta^{3/10})$ and the width is $O(R\delta^{3/5})$, which is a negligible proportion of the whole. It is puzzling that, with these scalings, the dissipation associated with the side regions should be $O(\delta^{2/5})$ relative to the dissipation in the Landau–Levich regions (Hodges *et al.* 2004), whereas the numerical solutions only show an $O(\delta)$ correction to the speed. We do not understand this discrepancy.

4.3. *Growth towards dripping*

We conclude our discussion of translation over a uniform layer by noting that the thin-film theory predicts a finite-time blow up in the amplitude of the drop. Since $V \propto A$, $\mathrm{d}V/\mathrm{d}t \propto c$ from (4.5) and $c \propto A^{3/2}$ from (4.20), we find that $\mathrm{d}A/\mathrm{d}t \propto A^{3/2}$. Thus

$$A = A_0(1 - t/t_*)^{-2}, \tag{4.22}$$

where A_0 is the initial amplitude and t_* is the blow-up time. Inclusion of the constants in this calculation gives

$$t_* = (3\pi R/\gamma C^{3/2})h_+^{-5/2}A_0^{-1/2} = 427 h_+^{-5/2}A_0^{-1/2}, \tag{4.23}$$

which shows the dependence on the film thickness and initial amplitude.

Before blow-up can occur the thin-film approximation of the curvature κ by $\nabla^2 h$ breaks down. The calculation can be continued by modifying the governing equation (2.4) to include the full curvature. Though lubrication theory is not strictly valid within the drop when its dimensional amplitude becomes comparable to its radius, the modified equation predicts the correct quasi-static equilibrium for the interior of the drop and the propagation speed is set by the thin regions at the edge

where lubrication theory is valid. The asymptotic analysis of propagation can thus be modified by matching the Landau–Levich regions to the basal radius and curvature of a finite-amplitude pendent drop. We conclude that the drop continues to propagate and increase in volume until, in finite time, the stability limit of a pendent drop is exceeded and part of the drop drips off the ceiling. We anticipate that the remainder will re-equilibrate into a smaller drop and then continue to propagate and grow until it forms another drip. In principle, on an infinite, perfectly uniform film there could be periodic episodes of propagation and dripping. In practice, however, t_* may not be much less than the $O(h_+^{-3})$ time scale for growth of disturbances to the uniform film and so the main drop would eventually find itself propagating into a region where smaller drops were already growing.

4.4. *Translation over a slowly varying layer*

Motivated by the observation that the film ahead of a translating drop may already have undergone some disturbance, we now consider a drop propagating over a film of slowly varying thickness $h_+(x, y, t)$. By 'slowly varying' we mean: first, that the horizontal variations of h_+ are on a length scale much greater than the Landau–Levich length scale δ of the ring around the drop, which is the case for the natural linear instability of the film; and second, that the temporal variation occurs on a much longer time scale than that of translation of the drop, which will be true if $h_+ \ll A$. In these circumstances, it is relatively straightforward to generalize the analysis of uniform translation to that of a drop travelling with speed $c(t)$ at an angle $\theta_c(t)$ to the x-axis over such a slowly varying film.

Let $h_+(\theta)$ denote the film thickness just ahead of the drop in $\theta_c - (\pi/2) < \theta < \theta_c + (\pi/2)$ and $h_-(\theta)$ the thickness left in the wake. Let $\phi = \theta - \theta_c$ denote the angle to the direction of motion. The Landau–Levich analysis of (4.8)–(4.15) then carries over with $\cos\phi$ replacing $\cos\theta$ throughout. The boundary condition on the Helmholtz problem for the quasi-static drop shape must have no terms in either $\cos\theta$ or $\sin\theta$. Hence there are two solubility criteria, which can be written as

$$A\int_{-\pi/2}^{\pi/2} h_+(\phi+\theta_c)b_+[\lambda(\phi;c,\theta_c)]\cos\phi\,d\phi = a_-b_-\int_{-\pi/2}^{\pi/2}(3c\cos\phi)^{2/3}\cos\phi\,d\phi, \quad (4.24)$$

$$A\int_{-\pi/2}^{\pi/2} h_+(\phi+\theta_c)b_+[\lambda(\phi;c,\theta_c)]\sin\phi\,d\phi = 0, \quad (4.25)$$

where $\lambda(\phi;c,\theta_c)$ is given implicitly by

$$a_+(\lambda) = Ah_+(\phi+\theta_c)(3c\cos\phi)^{-2/3}. \quad (4.26)$$

In principle, (4.24) and (4.25) determine c and θ_c. In particular, the factor $\sin\phi$ in (4.25) shows that the drop moves in such a way that a certain average thickness on the left-hand side of the direction of motion is equal to that the right-hand side. If h_+ is slowly varying and (4.24) and (4.25) are satisfied throughout the motion of the drop then θ_c should in general vary continuously. Hence we anticipate that one would need to consider the variation of the conditions (4.24) and (4.25) along the instantaneous direction of travel in order to determine the rate of change of direction $\mathrm{d}\theta_c/\mathrm{d}t$ of a curving trajectory. From this information one could then integrate along the trajectory. (We have not worked through the details of this calculation.)

Since release of gravitational potential energy is the driving mechanism for translation, we expect the drop to veer towards regions where the film thickness is greater. (For example, if h_+ varies slowly even on the length scale R of the drop

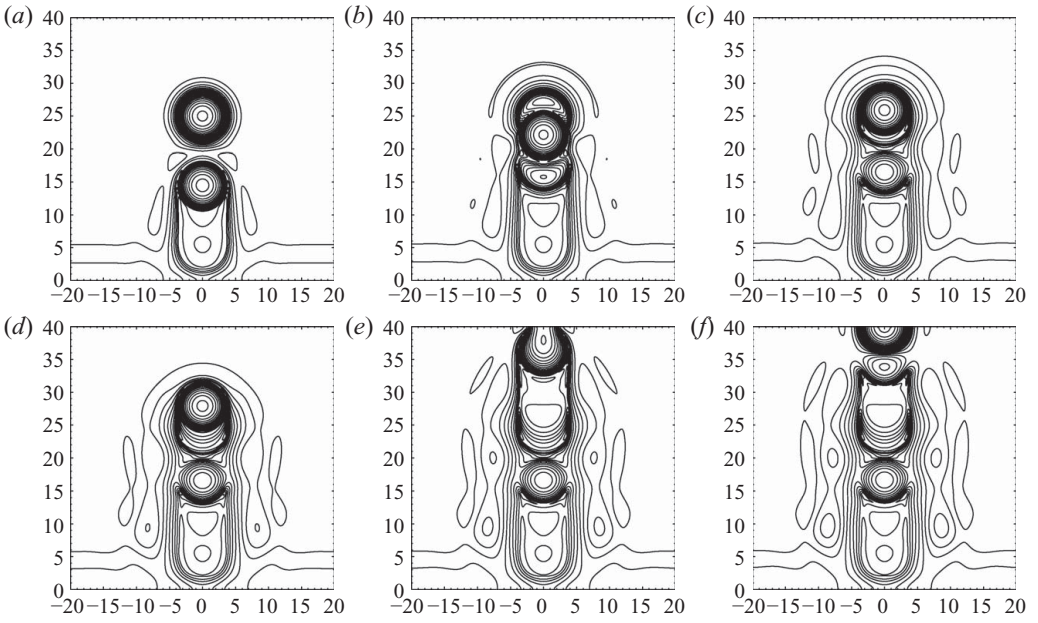

FIGURE 7. Collision of a moving drop with unit initial height with an equal stationary drop sitting on a film of thickness 0.025. The contours are at values $2^{i/2}$ in (a)–(f). The times are given by $10^{-6}t = 0.37, 0.57, 0.78, 0.87, 0.96$ and 1.07 respectively.

then (4.25) shows that the drop must move in the same direction as the local value of ∇h_+.) Sample numerical calculations confirm the tendency of a drop to veer towards greater film thicknesses, and this simple idea can be used to understand most of the complicated behaviour during collisions that is described in the following section. We note that the reduced film thickness in the wake produced by previous motion provides a strong bias for a drop to continue moving in the same direction once started.

5. Collisions of drops with drops and wakes

Having established that a single drop can translate over an otherwise uniform film, we now use illustrative numerical simulations to describe the dynamics of collisions between drops or between a drop and a wake. A drop of unit height was set in motion towards some sort of 'target' using a ramp of similar form to (4.1*b*). The orientation of the ramp determines the initial direction of motion, and the initial film thickness between the ramp and the target was 0.025. As we show below, there are rich dynamics to explore in such problems. We have not sought detailed asymptotic solutions to explain all the phenomena seen, and suspect this would be a considerable challenge.

5.1. *Head-on collision with a stationary drop*

Figure 7 shows a head-on collision between a moving drop and a stationary drop of equal amplitude. During the period before the collision, a circular trough or 'moat' develops around the stationary drop owing to drainage from the surrounding film into the lower-pressure drop. Weaker concentric circular peaks and troughs form around the moat. As the moving drop approaches, it speeds up and slows down as it encounters these peaks and troughs. As it reaches the moat (figure 7*a*), it slows down

significantly, and a single U-shaped minimum forms and deepens near the point of contact between the drops. However, forward motion continues. The minimum splits and the new minima move sideways away from the point of contact, while the film thickness near the point of contact starts to increase rapidly, and the drops coalesce (figure 7*b*). The rapid forward motion during coalescence leaves a thicker region in the wake (cf. (4.13)), which subsequently forms a daughter drop of height 0.09 behind the main coalesced drop of height 2.26 (figure 7*c*). After coalescence, the main drop continues its forward motion until, in this simulation, it collides with the boundary at $y = 40$ (figure 7*d*) and coalesces with the mirror image drop that is implied in $y > 40$ by the symmetry boundary conditions (2.5). The processes of collision and coalescence with the image drop are very similar to those with the stationary target drop.

The most interesting result from this simulation is that coalescence of colliding drops can and does occur. Colliding collars, governed by the one-dimensional version of (2.4), do not coalesce because the neck between the collars thins rapidly like t^{-1} and the forward motion consequently slows like $t^{-3/2}$ (Lister *et al.* 2006*b*). In the present two-dimensional calculation, while the layer does thin to less than 0.001 near the point of contact, the drop continues to be propelled forwards, presumably by the layer-eating mechanism around the rest of its perimeter, and its velocity falls by only a factor of 10 from the free speed (and not by the much larger factor $(0.025/0.001)^{3/2}$ that would result in one dimension). Eventually, a fully two-dimensional motion eliminates the moat between the drops, which coalesce. Given the difference from the one-dimensional behaviour, it is worth emphasizing that coalescence is not an artefact of inadequate numerical resolution between the colliding drops: for example, checks such as halving the grid spacing did not delay coalescence, reduce the minimum thickness near the point of contact or affect the variations in forward velocity.

5.2. *Oblique collisions with stationary drops and wakes*

Figure 8 shows a collision between a moving drop and a stationary drop of equal amplitude, in which the initial path of the moving drop is offset from the centre of the stationary drop by a distance $0.5R$. The approach towards collision (figure 8*a,b*) is essentially the same as with a head-on collision. However, as the moat around the stationary drop deepens locally into a U-shaped trench between the drops, impeding the forward motion towards coalescence, the moving drop find it easier to move sideways towards thicker parts of the layer, and the drop ricochets off at a tangent (figure 8*c,d*). On reaching the boundary $x = 20$, the drop coalesces with its mirror image and, somewhat surprisingly, the combined drop moves back along boundary towards $y = 0$.

Figure 9 shows a similar collision, but with initial offset $3R$. It might have been expected that, with this offset, the moving drop would miss the 'target'. However, the moving drop is deflected by attraction towards a weak peak concentric with the moat around the stationary drop (figure 9*b*), and then undergoes a complex series of interactions with the stationary drop and with the boundaries (figure 9*c–f*). The tangential deflection off the drop (figure 9*c*) occurs by the same mechanism as that discussed for offset $0.5R$. Note that the moving drop does not coalesce with its image on collision with the boundary $y = 40$ (figure 9*d*), but bounces off and continues on to coalescence with its image in the boundary $x = -20$ (figure 9*e*).

Figure 10 shows collision with a wake-like feature lying at 45° across the path of the moving drop. The wake was created artificially by reducing the initial film thickness within it by 90 %. During the period before the collision, the edge of the

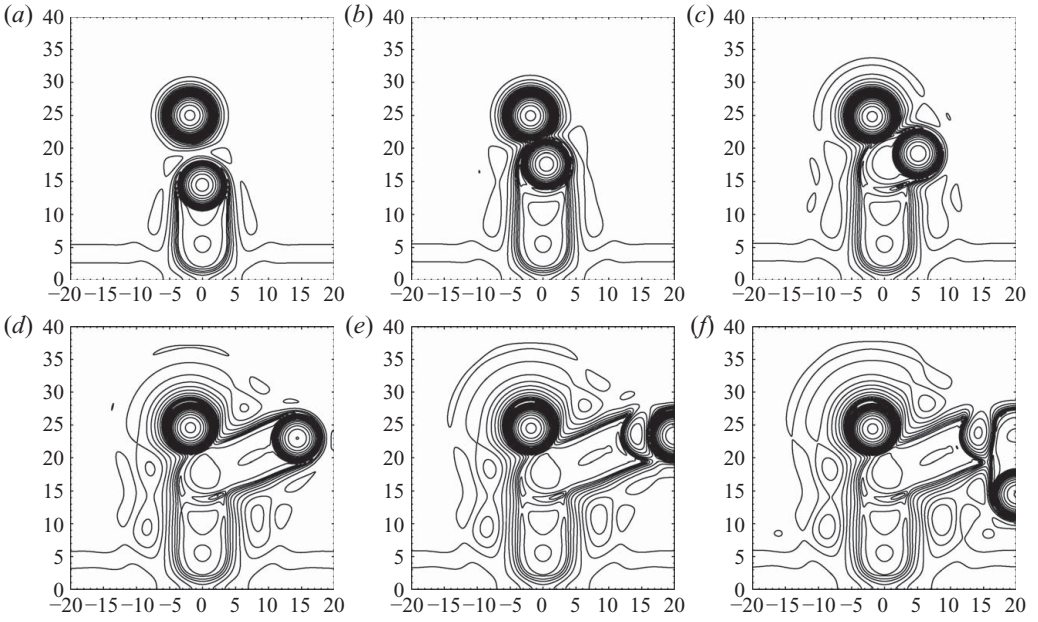

FIGURE 8. Collision with offset $0.5R$ at $10^{-6}t = 0.37, 0.53, 0.67, 0.93, 1.01$ and 1.11 in (a)–(f) respectively. The drop heights, film thickness and contour values are as in figure 7.

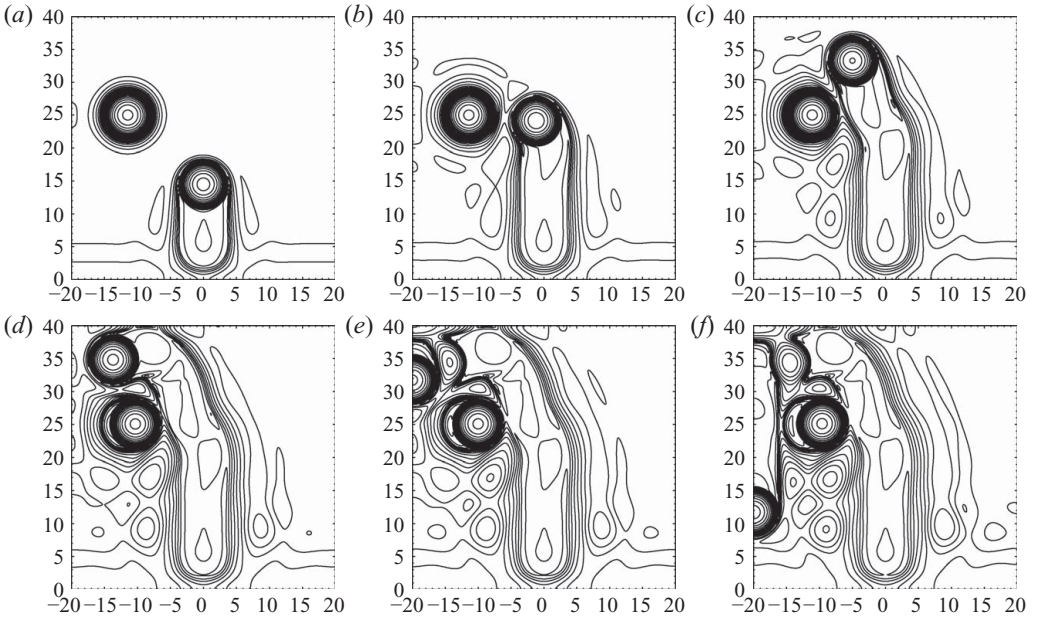

FIGURE 9. Collision with offset $3R$ at $10^{-6}t = 0.38, 0.66, 0.90, 1.09, 1.18$ and 1.33 in (a)–(f) respectively. The drop heights, film thickness and contour values are as in figure 7.

wake smooths off and develops weak marginal ridges and troughs so that it has a cross-section similar to that of a real wake (figure 5*b*). The moving drop is deflected towards the wake by the largest of these peaks (figure 10*b*), and then sideways, tangential to the wake, by the impediment provided by the thin film in the wake

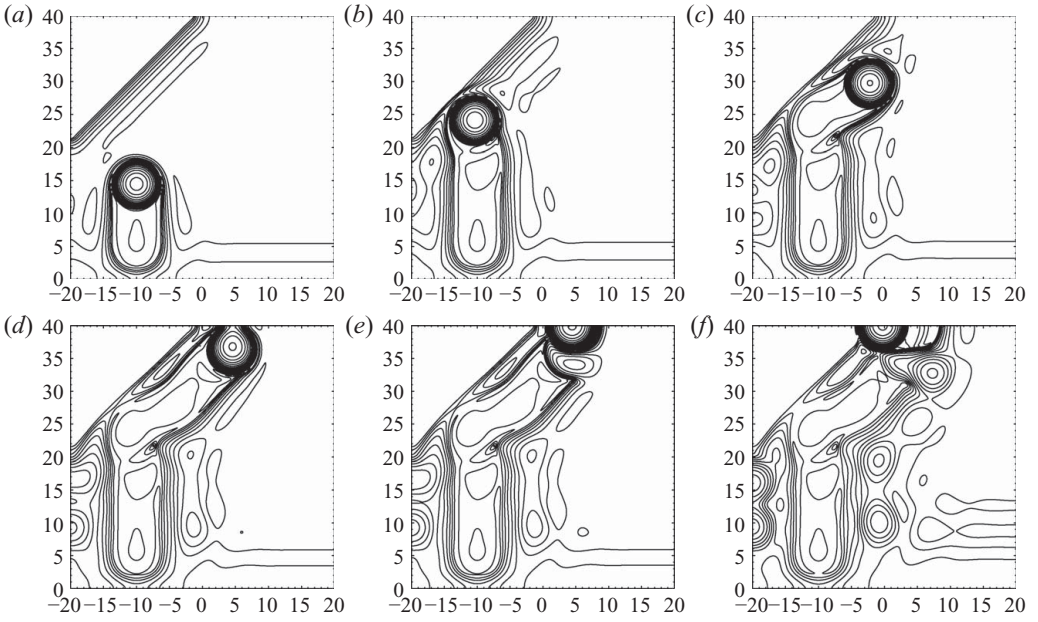

FIGURE 10. Collision at 45° with an artificial wake of thickness 0.0025 in a film of thickness 0.025. The times are $10^{-6}t = 0.38, 0.68, 0.90, 1.09, 1.14$ and 1.63 in (a)–(f) respectively. The contour values are as in figure 7.

to continued forward motion (figure 10*c*,*d*). The retrograde motion after coalescence (figure 10*f*) is again somewhat surprising. Even though the drop starts progressing into the artificial wake, it leaves an even thinner film behind so that, once established, the direction of motion is maintained.

5.3. *Oblique collisions of moving drops*

In § 5.2 we showed that moving drops are deflected by the capillary waves that surround stationary features, while coalescence usually, but not always, occurs when a drop collides with its image in a boundary. To investigate this further, we used an angled ramp to impel a drop towards its image in the boundary $x = 20$ at various angles of incidence. For these calculations we also used a similar strategy to that of § 4.1 to allow indefinite translation in the y direction.

Figure 11(a) shows the trajectories of the maximum for each of four such drops. At incident angles to the boundary steeper than about 25° (one example shown) the drop coalesces with its image. Over a range of shallower incident angles (two examples shown) the drop is deflected by interactions with its image to settle, after a series of damped oscillations, into motion almost parallel to the boundary at $x = 10$. At the shallowest incident angle shown the drop bounces back from the boundary at $x = 10$, collides at a slightly greater angle with the boundary at $x = -10$, and settles into motion almost parallel to this boundary.

The slight deflections towards and away from the boundary, which can be seen as the trajectories approach it, can be explained as attractions and repulsions by the peaks and troughs of the capillary wave field ahead of the image drop. This wave field reflects the oscillatory nature of the solution $H_+(\xi)$ to the Landau–Levich equation (4.10), and is shown in figure 11(b) for a single drop. We hypothesize that the separation between a drop and its image in solutions where they move along a

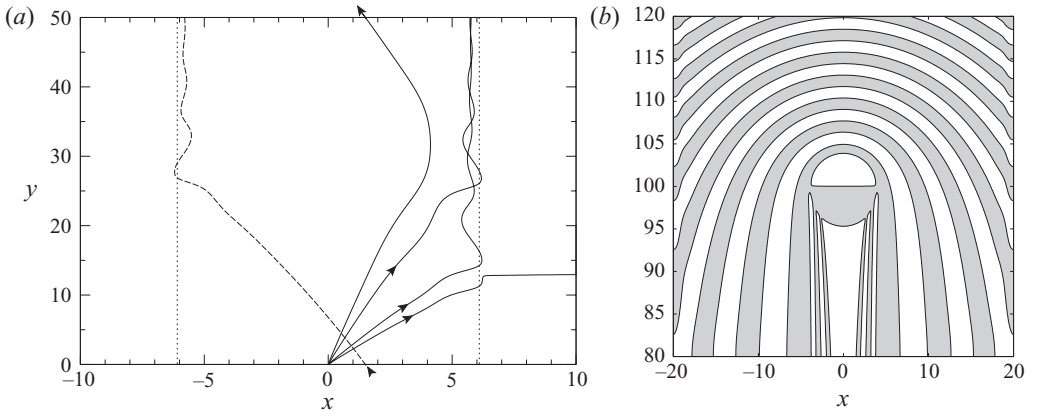

FIGURE 11. (*a*) Trajectories of the maximum of a moving drop relative to its initial position on a domain $-20 \leqslant x \leqslant 20$ for four initial directions of motion. (The dashed line shows the continuation of one trajectory shifted back by 50.) The dotted lines are at $|x| = 20 - R$. (*b*) The contour $h_t = 0$ for a single drop shows the capillary wave field generated ahead of the drop and shed to the side. The amplitude of h_t decreases exponentially away from the drop.

boundary together is related to the width of the first capillary wave at the side of the drop. If this is the case then we conjecture that there may be other solutions, less stable and harder to find, in which there are several capillary ridges between the drops.

The three trajectories that settle into motion almost parallel to the boundary, and others not shown in figure 11(*a*), have a number of features in common. The point of closest approach on the first oscillation is slightly less than R from the boundary but the distance after the oscillations die down is slightly greater than R. As can be seen in the figure, for a given amplitude of drop A and layer thickness h_+, the oscillations have approximately the same wavelength and damping rate. Presumably, this could be found through a linear stability calculation about a translating doublet solution for the drop and its image. After the oscillations have died away (or been subtracted by data analysis), the remaining distance δx by which the drop exceeds a distance R from the boundary slowly decreases as the drop propagates along the boundary while the amplitude of the drop increases. Comparison of the numerical data from several runs suggests that $\delta x \propto [h_+/A(t)]^{0.40\pm0.05}$. For comparison, the scaling of the Landau–Levich region is $(h_+/A)^{1/2}$, though we note that this scaling breaks down at the sides of the drop.

6. Discussion

We have shown in this paper that the dynamics of pendent drops on a thin film coating the underside of a ceiling depend on the horizontal extent of the film through the constraints exerted by the boundary conditions at its edge. A small film is stabilized by surface tension since there is no room for the gravitationally unstable wavelengths. On a long, narrow rectangular film, the evolution tends towards that of the analogous one-dimensional problem (Lister *et al.* 2006*a*, *b*) with vanishing variation across the narrow dimension. On films of moderate horizontal extent, the pendent drops are pinned by the boundary conditions and the intervening film drains slowly into the drops. In this case the evolution becomes self-similar, with the same temporal scalings

as the one-dimensional problem (Hammond 1983), but with azimuthal variations around the perimeter of the drop and coefficients that depend on the plan-form of the intervening film. On a film of large horizontal extent, pendent drops can undergo self-sustained translation, as in one-dimension, driven by accumulation of fluid from the film into the drop. Colliding drops display complex dynamics and, unlike the one-dimensionsional analogues, can coalesce.

Experimental observations of translating drops would be of great interest. In the experiments of Fermigier *et al.* (1992) and Limat *et al.* (1992) an array of drops was allowed to develop from an almost uniform film, and the array was almost completely pinned either by the packing of drops inward from the boundaries or by fixed heterogeneities (dust or wires) that triggered the instability. In order to realize the translating-drop solutions, we suggest that a finite-amplitude drop should be placed on a very uniform and thin film so that there is time to observe translation before the film develops its instability. We note that, in units of time $\mu\ell^4/\sigma h_+^3$, the time $2R/c$ for translation by one diameter is $1600(h_+/h_d)^{3/2}$ and the exponential growth time for the layer is 12. Hence one needs h_d/h_+ to be large. It is also likely to be necessary to initiate translation in a particular direction, as with the ramp in §4, perhaps by towing the drop a short distance with a pipette. Without an initial symmetry breaking disturbance, the drop would remain stationary and simply act as a nucleation point for the film instability and subsequent front propagation.

From a theoretical point of view, many questions revealed by our study remain to be explored, particularly regarding the rich dynamics of colliding drops and the trajectories of drops on non-uniform films. Detailed investigation of the criteria for coalescence, doublet formation and bouncing off during collision in terms of the amplitudes and impact parameters of the drops is beyond the scope of this paper, as is the long-term statistics of many-drop interactions. Some of these problems are reminiscent of the complex dynamics of drops bouncing on Faraday waves (e.g. Protiere, Bohn & Couder 2008) though the physical systems seem quite different. Finally, we note that there are many generalizations of thin-film equations (see e.g. Oron, Davis & Bankoff 1997; Bertozzi & Pugh 1998; King & Bowen 2001; Weidner, Schwartz & Eres 2007) to include van der Waals forces, mobility coefficients h^n with $n \neq 3$, Marangoni effects, evaporation or slip. Much of the theory developed for these problems in one dimension could now be re-examined to explore the possibilities for drop-like dynamics in two dimensions.

It is a pleasure to contribute a paper on capillary-driven thin-film flow to a volume in honour of Steve Davis. We have benefited greatly from Steve's many seminal contributions to this area of study. The challenge of including thermocapillarity in our problem must, alas, await another occasion. S. J. R. was supported by a summer studentship from Trinity College, Cambridge.

Appendix. Numerical discretization

Most of our numerical solutions of (2.4) were calculated using an ADI method proposed by Witelski & Bowen (2003), which we found performed better than a conjugate-gradient method with a fully implicit pressure discretization. This appendix gives further details of the two methods.

A.1. *ADI method*

Witelski & Bowen (2003) review and test a variety of ADI schemes for the solution of fourth-order nonlinear diffusion equations such as (2.4). For simplicity, we chose

the non-iterated version of the scheme they denote (pL_1) (pseudolinear, first order in time). This can conveniently be written symbolically as a 'factorized' set of equations

$$\mathscr{L}_x w = -\tfrac{1}{3}\Delta t\, \nabla\cdot\left[f(h^{(n)})\nabla\left(\nabla^2 h^{(n)} + h^{(n)}\right)\right], \tag{A 1a}$$

$$\mathscr{L}_y v = w, \tag{A 1b}$$

$$h^{(n+1)} = h^{(n)} + v, \tag{A 1c}$$

which are then solved in sequence to time step by Δt from $h^{(n)}$ to $h^{(n+1)}$. Here $\mathscr{L}_x$ and $\mathscr{L}_y$ are linear differential operators defined by

$$\mathscr{L}_x \cdot = 1 + \tfrac{1}{3}\Delta t\, \partial_x[f(h^{(n)})\partial_x(\partial_{xx} + 1)\cdot], \quad \mathscr{L}_y \cdot = 1 + \tfrac{1}{3}\Delta t\, \partial_y[f(h^{(n)})\partial_y(\partial_{yy} + 1)\cdot], \tag{A 2}$$

and $f(h) = h^3$. The effect of solving (A 1*a–c*) is revealed more clearly by combining the equations to obtain, after some manipulation,

$$\begin{aligned}\frac{h^{(n+1)} - h^{(n)}}{\Delta t/3} = {} & -\partial_x\left(f^{(n)}\partial_x\left(\partial_{xx}h^{(n+1)} + h^{(n+1)}\right)\right) - \partial_y\left(f^{(n)}\partial_y\left(\partial_{yy}h^{(n+1)} + h^{(n+1)}\right)\right) \\ & - \partial_x\left(f^{(n)}\partial_{xyy}h^{(n)}\right) + \partial_y\left(f^{(n)}\partial_{yxx}h^{(n)}\right) + O(\Delta t^2).\end{aligned} \tag{A 3}$$

(The $O(\Delta t^2)$ correction arises from the $O(\Delta t^2)$ part of $\mathscr{L}_x\mathscr{L}_y$.) Thus the scheme is similar to (2.11), but with the mixed-derivative terms treated explicitly instead of implicitly. Witelski & Bowen (2003) note that, with a small modification, (A 1) could be iterated at each time step, replacing occurrences of $h^{(n)}$ by successive estimates of $h^{(n+1)}$, to obtain an implementation of a fully implicit backward-Euler scheme. However, they and we both found that iteration did not noticeably improve the accuracy or stability of the scheme, and is therefore not worth the extra computational cost.

Having factored the time evolution into the form (A 1), it is now straightforward to represent the spatial derivatives in (A 1) and (A 2) in the standard way by centred finite differences on an evenly spaced rectangular grid. Following the recommendation of Witelski & Bowen (2003) and Zhornitskaya & Bertozzi (2000), the required midpoint values f_{12} between values h_1 and h_2 on neighbouring grid points were defined by

$$f_{12} = \frac{2h_1^2h_2^2}{h_1 + h_2} = \frac{h_1 - h_2}{F(h_1) - F(h_2)}, \quad \text{where} \quad F(u) = \int \frac{\mathrm{d}u}{f(u)}. \tag{A 4}$$

(We found that sample calculations with the more obvious definitions $(h_1^3 + h_2^3)/2$ or $[(h_1 + h_2)/2]^3$ gave essentially the same results.)

On discretizing $\mathscr{L}_x$ and $\mathscr{L}_y$, (A 1*a*) and (A 1*b*) each reduce to a set of linear pentadiagonal systems, which are easily inverted for w and v. The boundary conditions (2.5) are implemented by extending the mesh by an extra two grid points around the whole domain and allocating or enforcing the necessary mirroring values from within the domain.

The whole procedure offers second-order accuracy in space and first-order accuracy in time. The grid spacing was typically about 0.04. Time steps were chosen adaptively such that h did not change by more than about 0.2 % at any point. (The spacing and time-step control were both varied to check the accuracy of the results.) The scheme breaks down at very long times owing to a loss of resolution or a loss of stability as the solution develops very narrow and slowly evolving features, but the results presented are well before this time.

A.2. *Conjugate gradient method*

In an attempt to use larger time steps than the ADI scheme would permit, we tried the fully implicit treatment (2.11) of the pressure field. To invert the resultant sparse non-symmetric banded matrix we used a bi-conjugate gradient method, with the diagonal of the matrix as a preconditioner. In configurations for which a self-similar structure developed (see § 3) this technique did indeed permit large time steps Δt proportional to t to be taken under the requirement that the largest fractional change in h should not exceed 0.2 % in any step. Furthermore, the step-controlling points were in regions of small h rather than large h, exactly as expected and in agreement with the one-dimensional simulations. The difficulty with the method, however, is that the sparse matrix is solved iteratively. For an $N \times N$ system using exact arithmetic, convergence is guaranteed in N iterations. We found that starting from the (good) solution guess given by the ADI method, about $N/2$ iterations of the algorithm were still needed, and that this number grew slowly as Δt increased (presumably because the matrix becomes increasingly ill-conditioned) until, owing to a lack of machine accuracy, the algorithm no longer converged. (On a grid with spacing 0.1, convergence to a self-similar solution was possible for values of Δt up to about 30, which corresponds to a time t of order 10^4.) Unfortunately, too, it appears to be the smallest separation of computational nodes for an unevenly spaced grid that determines the condition number of the matrix and hence the speed of convergence.

We attempted to improve the algorithm by incorporating the ADI technique as a preconditioner for the conjugate-gradient method. This was unsuccessful for two reasons. First, when Δt is not small the split operator no longer provides a good approximation to the true matrix. More importantly, this preconditioned matrix 'spreads' the error across both thick and thin areas of the film and this leads to solutions that are no better than using the ADI algorithm itself; the time step is again restricted to be small compared with unity and is controlled by the thicker areas of the film.

We concluded that, in the absence of a better preconditioner for the bi-conjugate gradient method, the ADI method is more robust, and no more expensive overall, and we have used it in the results presented.

REFERENCES

Bertozzi, A. L. & Pugh, M. C. 1998 Long-wave instabilities and saturation in thin film equations. *Commun. Pure Appl. Math.* **51**, 625–661.

Bretherton, F. P. 1961 The motion of long bubbles in tubes. *J. Fluid Mech.* **10**, 166–188.

Burgess, D. & Foster, M. R. 1990 Analysis of the boundary conditions for a Hele-Shaw bubble. *Phys. Fluids* **2**, 1105–1117.

Chandrasekhar, S. 1981 *Hydrodynamic and Hydromagnetic Stability*. Dover.

Fermigier, M., Limat, L., Wesfreid, J. E., Boudinet, P. & Quilliet, C. 1992 Two-dimensional patterns in Rayleigh–Taylor instability of a thin-layer. *J. Fluid Mech.* **236**, 349–383.

Fetzer, R., Jacobs, K., Münch, A., Wagner, B. & Witelski, T. P. 2005 New slip regimes and the shape of dewetting thin liquid films. *Phys. Rev. Lett.* **95**, 127801.

Glasner, K. B. 2007 Dynamics of pendent drops on a one-dimensional surface. *Phys. Fluids* **19**, 102104.

Glasner, K. B. & Witelski, T. P. 2003 Coarsening dynamics of dewetting films. *Phys. Rev.* E **67**, 016302.

Gratton, M. B. & Witelski, T. P. 2008 Coarsening of unstable thin films subject to gravity. *Phys. Rev.* E **77**, 016301.

Hammond, P. S. 1983 Nonlinear adjustment of a thin annular film of viscous fluid surrounding a thread of another within a circular cylindrical tube. *J. Fluid Mech.* **137**, 363–384.

Hodges, S. R., Jensen, O. E. & Rallison, J. M. 2004 Sliding, slipping and rolling: the sedimentation of a viscous drop down a gently inclined plane. *J. Fluid Mech.* **512**, 95–131.

Hynes, T. P. 1978 Stability of thin films. PhD Thesis. University of Cambridge, Cambridge, UK.

Jensen, O. E. 1997 The thin liquid lining of a weakly curved cylindrical tube *J. Fluid Mech.* **331**, 373–403.

Jones, A. F. & Wilson, S. D. R. 1978 The film drainage problem in droplet coalescence. *J. Fluid Mech.* **87**, 263–288.

King, J. R. & Bowen, M. 2001 Moving boundary problems and non-uniqueness for the thin film equation. *Eur. J. Appl. Math.* **12**, 321–356.

Landau, L. D. & Levich, B. 1942 Dragging of a liquid by a moving plate. *Acta Physicochim. URSS* **17**, 42–54.

Limat, L. 1993 Instabilité d'un liquide suspendu sous un surplomb solide: influence de l'épaisseur de la couche. *C. R. Acad. Sci. Paris* **317**, 563–568.

Limat, L., Jenffer, P., Dagens, B., Touron, E., Fermigier, M. & Wesfreid, J. E. 1992 Gravitational instabilities of thin liquid layers – dynamics of pattern selection. *Physica* D **61**, 166–182.

Lister, J. R. & Kerr, R. C. 1989 The effect of geometry on the gravitational instability of a buoyant region of viscous fluid. *J. Fluid Mech.* **202**, 577–594.

Lister, J. R., Morrison, N. F. & Rallison, J. R. 2006*a* Sedimentation of a two-dimensional drop towards a rigid horizontal plane. *J. Fluid Mech.* **552**, 345–351.

Lister, J. R., Rallison, J. R., King, A. A., Cummings, L. J. & Jensen, O. E. 2006*b* Capillary drainage of an annular film: the dynamics of collars and lobes. *J. Fluid Mech.* **552**, 311–343.

Nettleton, L. L. 1934 Fluid mechanics of salt domes. *Bull. Am. Assoc. Pet. Geol.* **18**, 175–204.

Newhouse, L. A. & Pozrikidis, C. 1990 The Rayleigh–Taylor instability of a viscous-liquid layer resting on a plane wall. *J. Fluid Mech.* **217**, 615–638.

Oron, A., Davis, S. H. & Bankoff, S. G. 1997 Long-scale evolution of thin liquid films. *Rev. Mod. Phys.* **69**, 931–980.

Protiere, S., Bohn, S. & Couder, Y. 2008 Exotic orbits of two interacting wave sources. *Phys. Rev.* E **78**, 036204.

Selig, F. 1965 A theoretical prediction of salt dome patterns. *Geophysics* **30**, 633–643.

Vrij, A. 1966 Possible mechanism for the spontaneous rupture of thin, free liquid films. *Discuss. Faraday Soc.* **42**, 23–33.

Weidner, D. E., Schwartz, L. W. & Eres, M. H. 2007 Suppression and reversal of drop formation in a model paint film. *Chem. Prod. Process Model.* **2**, 1–30. doi:10.2202/1934-2659.1078.

Whitehead, J. A. & Luther, D. S. 1975 Dynamics of laboratory diapir and plume models. *J. Geophys. Res.* **80**, 705–717.

Witelski, T. P. & Bowen, M. 2003 ADI schems for higher-order nonlinear diffusion equations. *Appl. Numer. Math.* **45**, 331–351.

Yiantsios, S. G. & Higgins, B. G. 1989 Rayleigh–Taylor instability in thin viscous films. *Phys. Fluids* A **1**, 1484–1501.

Zhang, W. W. & Lister, J. R. 1999 Similarity solutions for van-der-Waals rupture of a thin film on a solid substrate. *Phys. Fluids* A **11**, 2454–2462.

Zhornitskaya, L. & Bertozzi, A. L. 2000 Positivity-preserving numerical schemes for lubrication-type equations. *SIAM J. Numer. Anal.* **37** (2), 523–555.